High-Pressure Methane Jet: Analysis of the Jet-Obstacle Interaction

Cristian Colombini

Department of Chemistry, Materials and Chemical Engineering "Giulio Natta", Politecnico di Milano, Italy.
E-mail: cristian.colombini@polimi.it

Valentina Busini

Department of Chemistry, Materials and Chemical Engineering "Giulio Natta", Politecnico di Milano, Italy.
E-mail: valentina.busini@polimi.it

The study of unplanned high-pressure gas releases is of paramount importance in the industrial safety framework because of the possible large consequences, both in case of flammable and toxic substances leakage. In addition, if an obstacle is involved in the release, it is known that the main effect on the jet behavior is the enhancement of the risk area. Pointing out the importance to consider the obstacle presence, among the various available numerical approaches, the sole reliable tool able to correctly model the scenario of a jet interacting with an obstacle seems to be the Computational Fluid Dynamics (CFD). This work lies in the context outlined through the examination of a realistic unignited high-pressure methane jet interacting with a realistic obstacle placed along its axis via CFD simulations: a stationary 65-bara unignited methane jet outflowing from a one-inch diameter hole and a medium size horizontal cylindrical tank are the building blocks of the realistic scenario. The aim is to deeply investigate how the distance between obstacle and jet orifice modifies the jet behavior. In particular, the final purposes are: i) to establish when the obstacle most influences the jet cloud extent and, ii) to assess when the obstacle influence expires. Moreover, a sensitivity analysis on the obstacle shape and size is conducted for comparison purposes.

Keywords: industrial safety, safety assessment, methane, high-pressure jet, obstacle influence, numerical models, CFD.

1. Introduction

A large part of industrial gases is normally in a compressed form. Therefore, an accidental release, which generally arises from a failure in the process or storage equipment, results in high-pressure jet yielding a wide toxic or flammable cloud. In the second case, if ignition occurs, the consequences can be relevant: as reported by Casal et al. (2012), due to the domino effect related to it, a jet fire may be among the industrial's most hazardous accidents, whose damages may involve both people, facilities and environment. It is clear, therefore, why the study of high-pressure gas releases became of great interest in the industrial and process safety framework. Examples of such an importance are given by the work of Busini et al. (2012) and Pontiggia et al. (2014), just to mention some. By referring to a common industrial plant, it is easy to find that equipments, structures or properties can be in the vicinity of a hypothetical source of a high-pressure jet: broadly speaking, it can be very common to have obstacles close to the leak. Attention should be payed, therefore, to the previous depicted scenario. In particular, the main reason that should focus the concerns is that, as reported by Hall et al. (2017), the jet behavior is significantly affected by the obstacle presence, specifically through the enhancement of the cloud extent (and so the flammable area involved) with respect to the case of no-obstacle situation (known as free jet case). In a previous work made by Colombini and Busini (2019), the non-desirable effect that a cylindrical tank, placed in the surrounding of an accidental release and acting as realistic industrial obstacle, has on the jet dimensions is clearly depicted. So, even though its prominent importance in the safety assessment, a not so spread literature is noticeable. By way of example, as regards numerical analysis, works are available focusing on the effect of lateral surfaces (Hourri et al. (2009); Benard et al. (2016)) or small front barriers (Houf et al. (2010); Middha et al. (2010); Busini and Rota (2014)). The common denominator among the cited works is that the only reliable numerical tool is the CFD. As reported by Batt et al. (2016), CFD is the sole utility able to properly account for geometry complexities, although, as stated in the work of Zuliani et al. (2016), the computational costs and the user knowledge demanded.

To the knowledge of the authors, only the previous work done by Colombini and Busini (2019) reports a follow-up about the common scenario of a 3D realistic industrial obstacle placed in the vicinity of a realistic high-pressure gaseous release.

Proceedings of the 29th European Safety and Reliability Conference.
Edited by Michael Beer and Enrico Zio
Copyright © 2019 European Safety and Reliability Association.
Published by Research Publishing, Singapore.
ISBN: 978-981-11-2724-3; doi:10.3850/978-981-11-2724-3_0467-cd

In the framework outlined, this work proposes the examination of a realistic unignited high-pressure methane jet interacting with a realistic obstacle placed along its axis. The aim was to assess, with respect to the distance between obstacle and jet orifice, both qualitatively and quantitatively the influence of such an obstacle on the jet behavior (*i.e.*, in terms of Lower Flammability Limit (LFL) area extent). Two are the leading questions of the work: i) when the obstacle most influences the jet cloud extents and, ii) when the obstacle influence expires. Practically, as first, the CFD model results will be compared to experimental data found in literature for the case of a stationary unignited high-pressure methane jet without any kind of obstacle for validation purposes. Then, both a realistic industrial gas source and a realistic industrial obstacle will be selected for the analysis: a stationary 65-bara unignited methane jet outflowing from a one-inch diameter hole and a medium-size horizontal cylindrical tank will be considered. Moreover, in order to extend the knowledge acquired about the jet-obstacle interaction, a sensitivity analysis on the obstacle size and on the obstacle shape will be conducted.

2. General Aspects of the CFD Models

As CFD software, Ansys® Fluent® release 19 was used to conduct the whole analysis. In particular, the Workbench suite was adopted due to its ease-to-use and bring-together design. The validation case, the case study and the sensitivity analysis studies share some aspects in terms of geometry, mesh and solver settings. With regard to the geometrical aspects, in all the models reported in the work, a nozzle was used to represent the methane inlet in the domain and a symmetry vertical plane along the jet axis was adopted. As first reference, the computational domain extents were sized according to the guidelines reported in the work of Baklanov et al. (2007) that suggests proper dimensions for a CFD computational domain in the case of single building struck by the wind. The employed mesh strategy had the goal of balancing the computational costs and the results' reliability: the body of influence mesh modeler feature was found to be a good compromise. Indeed, placing virtual line bodies along the jet axis and then playing with their number, edge cells size and growth rate of the cells dimension into the fluid volume, cells thickening along the jet axis and in correspondence to the orifice was achieved, leaving a coarser mesh far from the "critical" zone of the domain. In all the models, a full tetrahedral grid was adopted. Finally, with the previously discussed solver general aspects, all simulations were performed in steady state mode and utilizing the pressure-based solver type. The Navier-Stokes equations system that describes the fluid behavior was solved in the sense of the Reynolds average. By exploiting this easier formulation, it is possible to get an acceptable trade-off between time-saving and flow field reproduction quality. The k-ω SST turbulence closure model was chosen in order to take into account the turbulence's effect on the flow field avoiding, on the other hand, the need to precisely portray the boundary layer region next to the ground and obstacle surfaces (when present). For more details about the k-ω SST turbulence model, refer to the Ansys® Fluent® User guide (2018). To account for the multi-species problem (methane release in ambient air), the species transport model without any kind of reaction was included. The methane release was modeled as mass flow inlet boundary condition and, for the boundaries of the domain, an *ad hoc* strategy was implemented case-by-case (*i.e.*, depending on whether or not the wind presence should be considered). As pressure-velocity coupling scheme, the coupled was adopted while a 2nd order spatial-discretization scheme was considered for all the equations. Concluding, usually 1500 iterations were sufficient in all the simulations performed to obtain a converged solution.

3. Validation Case

As introduced in Section 1, first of all the CFD model was validated. The work of Birch et al. (1984), concerning an experimental campaign involving natural gas free jets at various pressures, was taken as reference for the results comparison. However, other than for matching purposes, this work was also relevant because it provides the so-called pseudo-diameter model: it consists in an analytical model that returns a diameter of a pseudo gas source whereby the mass flow rate is preserved but the supercritical conditions are replaced by critical conditions (*i.e.*, easier to be treated). In their work, the authors have shown that the Chen and Rodi (1980) axial concentration decay model, which is developed for sub-critical releases, can be also valid for super-critical ones as long as the actual diameter is substituted by the pseudo-diameter one. For further details, the reader can refer to the work of Birch et al. (1984). Hence, following the general aspects depicted in Section 2 and accordingly to the Birch's experiment conditions, the CFD model was set. Exploiting the same results visualization style as in Birch et al. (1984), wherein the reciprocal of the axial mole fraction (η) is plotted over a suitable dimensionless axial distance from the jet orifice (*i.e.*, *n*, number of actual orifice diameters properly scaled), Figure 1 shows the fulfilling comparison achieved between CFD results and

the experimental data (here reproduced through a Matlab® model that matches the Chen and Rodi (1980) axial concentration decay model with the pseudo-diameter model of Birch et al. (1984)).

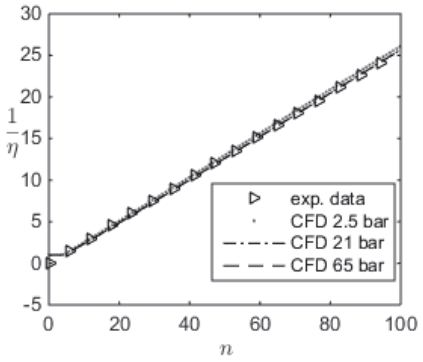

Fig. 1. Comparison of CFD results at three different pressures (namely 2.5, 21 and 65 bar) and experimental data.

Analyzing the matching shown in Figure 1, in the range defined by Birch et al. (1984) in which the model should be considered valid, no scatter between experimental data and CFD can be practically seen. Therefore, it is possible to conclude that the CFD model developed for the free jet scenario can be intended as validated.

4. Case Study

The case study, from which the analysis addressed in the present work started, was a stationary 65-bara unignited methane jet outflowing from a one-inch diameter hole impinging a medium size horizontal cylindrical tank. The realistic obstacle is 2.5 m long (in the symmetric domain), it has a diameter of 1.7 m and its longitudinal axis is 1 m high above ground. As anticipated in Section 3, the orifice diameter was sized using the Birch's pseudo diameter model: one-inch actual diameter and 65-bara of pressure give back a virtual source diameter equal to 0.1458 m, *i.e.*, almost 6 times the actual one. While, as regards the domain dimensions, according to what mentioned in Section 2, the domain extents were defined fulfilling the guideline of Baklanov et al. (2007). In particular, it was 10 m high, 10 m wide (in the symmetric domain) and 70 m long. The meshes built following the strategy illustrated in Section 2 resulted in good quality full tetrahedral grids whose elements number ranged between $4.94 \cdot 10^6$ and $5.64 \cdot 10^6$. Notice that, such a variation in the cells count is related to the obstacle position (with respect to the jet orifice) and the interaction of the cells face size on the tank surface with the cells edge size used for the bodies of influence placed along the jet axis. In the solver settings, the methane inlet was defined as a mass flow inlet boundary condition. In detail, a flow rate of 2.5924 kg/s and a total temperature of 344.3 K were the values assigned. Furthermore, since the scenario examined in the case study is outdoor located (contrary to the validation case depicted in Section 3, which is an indoor experiment), efforts were spent to define realistic wind conditions. In particular, a neutral atmospheric behavior with a wind intensity of 5 m/s at 10 m from the ground was considered. Therefore, to include in the solver the proper wind profile an *ad hoc* User Defined Function (UDF) was written. Lastly, to include the effect of an industrial ground surface on the wind field (*e.g.*, a concrete forecourt), a roughness height of 0.01 m was specified in the ground boundary condition dialog box.

From an operational point of view, to correctly investigate the influence of the distance between orifice and obstacle (D) on the jet behavior, two simulations were previously performed: i) a simulation (sim^{rif}) in which the Maximum Extent (ME in general, ME^{rif} in this case) of the LFL cloud was measured for the scenario wherein the obstacle was not placed in the domain (*i.e.*, the jet interacts only with the ground); ii) a simulation (sim0) in which the obstacle was placed at a distance correspondent to the half of ME^{rif}, namely D^0. Notice that, according to Colombini and Busini (2019), in addition to D there are three other geometrical key parameters which have to be set, that is to say: the height of the orifice above ground (H), the rotation (α) and the displacement (S) of the tank with respect to the jet axis. Therefore, the value issued for the four geometrical parameters used in sim^{rif} are the following: H = 1 m (H^{rif}), $\alpha = 0°$ (α^{rif}), S = 0 m (S^{rif}) and D = 53.7 m (D^{rif}). While, in sim0: $H = H^{rif}$ (H^0), $\alpha = \alpha^{rif}$ (α^0), $S = S^{rif}$ (S^0) and, consistently to what previously stated, D = 17.9 m (D^0). It is worth noting that H^{rif} was chosen equal to 1 m in order to have the orifice at the same height of the tank axis. Therefore, ME^{rif} is definitely linked to the height of the obstacle axis. To study the influence of D on the jet, a set of six simulations (sim1 to sim6) was performed. Table 1 lists the percentage variation with respect to D^0, δ, such as $D = D^0 + (\delta/100) \cdot D^0$ for each case. By way of example, let consider simulation 3 (sim3 in the table): D^3 is equal to $D^0 \cdot 1.25$, corresponding to D^3 = 22.375 m. It is worth noting that, in these six trials, the value of H, α and S was kept equal to the one used for sim0.

Prior to go through the results achieved, it has to be mentioned that the grid sensitivity analysis on the LFL cloud was successfully concluded. Indeed, using sim0 as check case, the results obtained with an initial mesh of about $5.54 \cdot 10^6$

elements are comparable with those produced by two other meshes of about $4 \cdot 10^6$ and $6.85 \cdot 10^6$ cells.

A qualitative way to evaluate the results is to plot the LFL isosurface. By way of example, Figure 2 shows the LFL cloud outline obtained from the results of sim3. In particular, Figure 2a shows a 3D view while Figure 2b shows a side view. Mostly from Figure 2b, although the relatively small height from the ground, it is possible to appreciate that most of the gas (for molar fractions larger than the LFL) goes beyond the tank passing below it. In general, it is also appreciable the role of the ground in the enhancement of the jet cloud due to its reflection effect. On the other way around, a quantitative assessment of the influence of the medium size horizontal cylindrical tank distance on the jet cloud can be obtained plotting the *ME* of the LFL clouds over δ. Figure 3 shows these information gathered from sim^{rif}, sim0 and the six trials listed in Table 1. By the findings shown in Figure 3, what deduced from Figure 2 is confirmed: the ground presence increases the jet length. In particular, the more the obstacle is far from the orifice and the more the ground influence progressively dominates. This last sentence allows to state that, in such a scenario, the obstacle plays as a barrier, whose effect opposes to the ground one. Finally, referring to the results of sim2 and sim^{rif} in Figure 3, it is noticeable that *ME* is practically the same, meaning that, at *D* obtained with δ = +50 %, the tank effect on the jet cloud is expired.

Table 1. δ values in the six trials.

Simulation	δ (%)
sim1	+75
sim2	+50
sim3	+25
sim4	-25
sim5	-50
sim6	-75

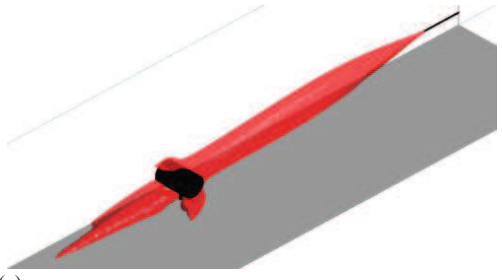

(a)

(b)

Fig. 2. 3D view (a) and side view (b) of the LFL cloud outline obtained from the results of sim3.

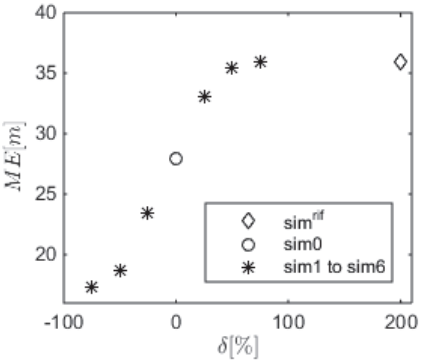

Fig. 3. Quantitative evaluation of the effect of the obstacle on the jet cloud: *ME* over δ trend.

5. Sensitivity Analysis

In the sensitivity analysis, substantially only the obstacle (in terms of size and shape) was varied with respect to the case study previously outlined. Hence, what described in Section 4 about the geometry, mesh, solver settings and simulations plan (*i.e.* the six simulations reported in Table 1) is still valid for the simulations that will be depicted in the following. However, a change of the obstacle clearly means a different geometry. This fact implies, therefore, two main differences among the case study and the cases analyzed in the present Section:

- As remarked in Section 4, H^{rif}, ME^{rif} and D^0 are linked to the obstacle dimensions. This means that, changing the obstacle leading to new values of *H* and *D* for both sim^{rif} and sim0
- Although the mesh strategy is the same as the one described in Section 4, a different obstacle causes a variation in the cells number.

As anticipated in Section 1, two are the kinds of sensitivity tested: the shape and the size of the obstacle. More in detail, for the size sensitivity a bigger horizontal cylindrical tank was considered while, for the shape sensitivity a vertical cylindrical tank which is of a size comparable to that of the case study's tank was considered. In

the two following Subsections, for both the sensitivity analysis conducted, geometries are described, and the results are presented.

5.1 *Obstacle size*

With respect to the case study, a bigger horizontal cylindrical tank was used to test the sensitivity of the results to the obstacle size. In particular, 2.4 m and 5.5 m (in the symmetric domain) are the diameter and the length considered, respectively, as real industrial dimensions. In this case, the height from ground of the tank axis is equal to 1.35 m. As anticipated, since the obstacle is different, new values of D and H for sim^{rif} and sim0 needs to be considered. Table 2 summarizes the four geometrical key parameters' value for both sim^{rif} and sim0.

Table 2. Values of H, α, S and D considered in sim^{rif} and sim0, respectively.

Simulation	H (m)	α (°)	S (m)	D (m)
sim^{rif}	1.35	0	0	42.225
sim0	1.35	0	0	14.075

With regard to the mesh cells count, placing along the jet axis this tank has led to grids with a number of elements belonging to a range of $8.61 \cdot 10^6$ and $10.2 \cdot 10^6$. To report one of the qualitative results achieved, by way of example, let consider the same simulation used in Figure 2 of the Case Study Section, *i.e.* sim3. Therefore, Figure 4 shows the LFL cloud outline correspondent to the case in which δ is equal to +25 %.

(a)

(b)

Fig. 4. LFL cloud contour by a 3D view (a) and a side view (b) obtained from the results of sim3.

From the figure, the jet shown has a similar shape as the one in Figure 2. Therefore, the qualitative considerations done for the case study can be extended to the scenario in which a bigger-size horizontal cylindrical tank is involved. By the quantitative point of view, in Figure 5 the *ME* of sim^{rif}, sim0 and the six simulations in which D is varied are plotted over δ. Figure 5 clearly depicts that the more the obstacle is far from the orifice and the more the jet stretches, meaning that the tank acts as barrier and, therefore, its effect is in opposition to the ground one. The obstacle effect, practically, expires when δ is between +50 % and +75 %.

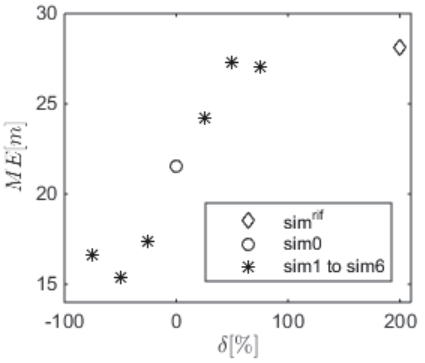

Fig. 5. Quantitative evaluation of the effect of the big-size horizontal cylindrical tank on the jet cloud.

5.2 *Obstacle shape*

The sensitivity analysis of the obstacle shape on the jet behavior was carried out considering a vertical cylindrical tank placed in front of the gas leak and varying its distance D. Comparable size with the horizontal one was considered. More precisely, the vertical tank was chosen with a diameter of 2 m and a length of 7 m, being these real industrial sizes. Notice that, in this case, the tank axis is vertically oriented. Therefore, to establish the jet height coherently to what has been done for the previous cases presented (*i.e.*, case study and obstacle size sensitivity analysis), the nearly mid-height of the obstacle was considered, giving H = 4 m. For the scenario here investigated, Table 3 reports the key parameter values for both sim^{rif} and sim0.

Table 3. Values of H, α, S and D considered in sim^{rif} and sim0 for the vertical cylindrical tank case.

Simulation	H (m)	α (°)	S (m)	D (m)
sim^{rif}	4	0	0	23.34
sim0	4	0	0	7.78

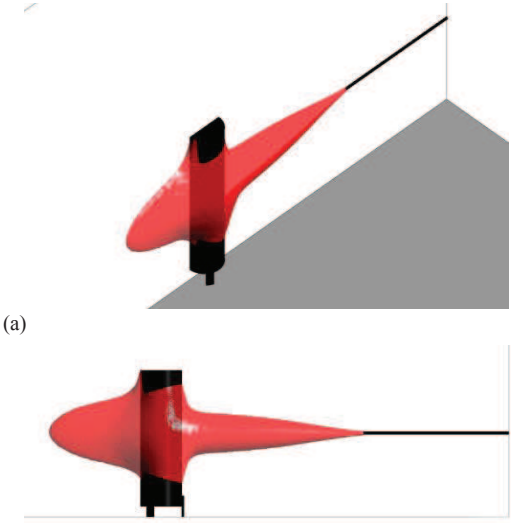

(a)

(b)

Fig. 6. LFL outline of sim3 of the shape sensitivity analysis: 6a) in a 3D view and, 6b) in a side view.

For what concerns the mesh dimensions, the number of the elements is within $4.5 \cdot 10^6$ and $4.7 \cdot 10^6$. Looking at the results, Figure 6 shows the LFL outline that is, by way of illustration, given by placing the vertical tank at a distance corresponding to $\delta = +25$ %, while, Figure 7 displays the *ME* over δ for sim^{rif}, sim0 and the six trials in which *D* was varied by a stepping δ of the 25 %, being $\delta \in [-75\ \%; +75\ \%]$. In Figure 6, it is evident that the obstacle, despite the different shape with regard to the one considered in Section 4, still continues to shorten the jet cloud, even thought, due to the increased jet height, in this case the LFL does not reflect against the ground surface. The latter effect is appreciable even by looking at Figure 7.

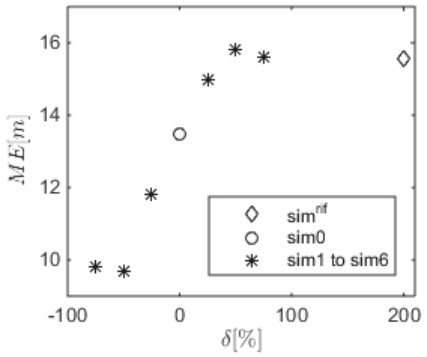

Fig. 7. *ME* over δ obtained from the vertical cylindrical tank case.

5. Results Comparison

Combining the results presented in Section 4 and 5, for different values of δ, the sensitivity of the obstacle shape and size effect on the jet evidently appears. In particular, from Figure 8 (wherein *ME* is plotted over δ), about the size effect it is possible to point out that:

- the results related to the case study Horizontal Cylindrical Tank (HCT_{CS} in the figure) and the bigger one considered for the sensitivity analysis (HCT_{SA} in the figure) present a similar behavior
- in both cases, an approximately straight section, wherein *ME* increases, is followed by a plateau, meaning constant values of *ME*
- quantitatively, for the two sizes involved, the slope of the results changes in correspondence of $\delta = +50$ % and the maximum value of *ME* is reached for $\delta \geq +50$ %: 35.88 m for the case of HCT_{CS} and 28.15 m for the case of HCT_{SA}
- a constant gap is present for values of $\delta \geq +50$ %, while a non-constant one for $\delta < +50$ %. The former can be related to the sole ground effect (where *H* is constant and, in particular, equal to the height of the cylindrical tank axis from ground, therefore *H* assumes different values for HCT_{CS} and HCT_{SA}), the latter can be caused by the obstacle-ground combined effect that can differ between the two sizes (giving, substantially, two different slopes).

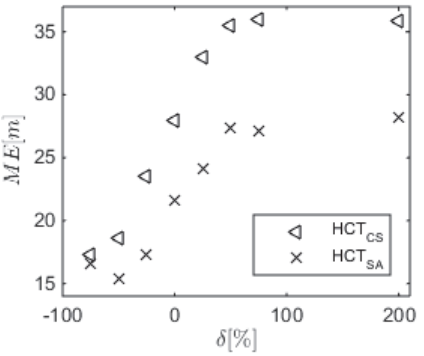

Fig. 8. *ME* over δ obtained varying the obstacle size.

The same goes for the shape effect, for which, from Figure 9 (wherein *ME* is plotted over δ), it is possible to say that:

- the results of the Vertical Cylindrical Tank used for the sensitivity analysis (VCT_{SA} in the figure) behave as the one of HCT_{CS}
- similar to the results obtained with the HCT_{SA}, an approximately straight section, wherein *ME* increases, is followed by a plateau even for the VCT_{SA} results where the obstacle no longer influences the jet
- quantitatively, for both shapes, the plateau of the *ME* is reached in correspondence of $\delta = +50$ %. Moreover, for the same δ, there is also the maximum value of *ME* (which is then kept for $\delta > +50$ %). For the VCT_{SA} case, the maximum *ME* is equal to 15.56 m
- a quite large constant gap is present for values of $\delta \geq +50$ %, while a non-constant one for $\delta < +50$ %. The possible causes previously depicted for the size influence analysis can deemed to be still valid.

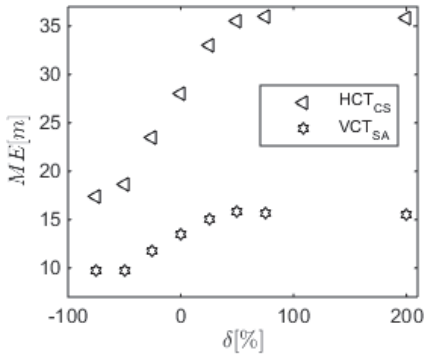

Fig. 9. *ME* over δ obtained varying the obstacle shape.

Finally, to profitably analyze the results all at once, a new graph was considered. In Figure 10, all the results are indeed collected and plotted in terms of Δ*ME* over δ. While the *x*-axis is the same as the one used up to this point, the *y*-axis is here defined as $\Delta ME = (ME^{rif}\text{-}ME)/ME^{rif}$, where ME^{rif} is the cloud Maximum Extent obtained in sim^{rif} while *ME* is the cloud Maximum Extent obtained in each of the simulations performed. As well as the simulations results, in Figure 10, a dashed line is also shown corresponding to $\Delta ME = 5$ %. This set threshold can be acceptable, for all the scenarios here addressed, since it corresponds to a little absolute jet *ME* variation with respect to ME^{rif}, *i.e.* lower than 2 m. So, concerning Figure 10, it is possible to state that:

- in a qualitatively perspective, all the results present a similar behavior
- the results compose two straight sections in which Δ*ME* decreases constantly or remains practically constant
- for all the findings, the slope change takes place at $\delta = +50$ %
- the results of the HCT_{CS} and HCT_{SA} present a Δ*ME* that often is similar, while the ones of VCT_{SA} are, for $\delta < +50$ %, always lower than the others. The cause can be mainly attributed to the smaller *H* in the VCT_{SA} scenario with respect to the one in both HCT_{CS} and HCT_{CS} scenarios.

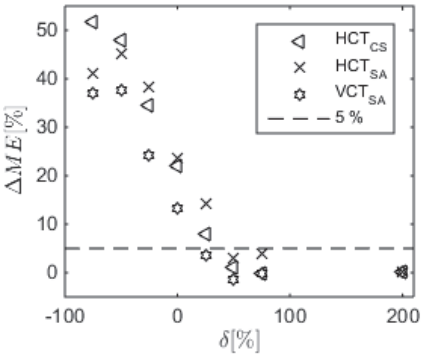

Fig. 10. Comparison of the *ME* obtained varying both size and obstacle shape: Δ*ME* over δ trend.

6. Conclusions

The scenario in which a 65-bara unignited methane gaseous jet that hits a realistic industrial obstacle is the focus of the present work. In particular, with respect to the distance between obstacle and jet orifice, the effect of a horizontal cylindrical tank of industrial use is considered on the jet LFL cloud. Moreover, with the purpose to understand how obstacle shape and size affect the jet behavior, a sensitivity analysis on these characteristics was conducted. Therefore, after validation of the CFD model with experimental data found in literature, the results of the depicted cases were obtained, and answer to the two leading questions was provided. More in detail:

- with respect to the jet orifice-obstacle distance (*D*), independently by size and shape, the obstacle acts as barrier, reducing the *ME* of the LFL cloud
- for all the cases investigated, the obstacle most influences the jet behaviour when it is placed as close as possible to the orifice (as

shown by Figure 10, ΔME reaches its maximum value)

- the obstacle influence can be intended as expired when $ME = ME^{rif}$. Considering ΔME = 5 % as an acceptable threshold, it was found that, for all the cases analyzed, the obstacle influence extinguishes for $\delta \geq +50$ %.

Finally, given that for $\delta \geq +50$ % the obstacle presence can be neglected, in those cases one can refers to simpler engineering correlations present in literature to assess the *ME* of the LFL cloud when the leak is close to plane surfaces (*e.g.*, the ground surface).

References

Ansys® (2017). Fluent User's Guide Release 18.2. ANSYS, Inc.

Baklanov, A., P. Barmpas, J. Bartzis, E. Batchvarova, K. Baumann-Stanzer, U. Berkowicz, C. Borrego, A. Britter, K. Brzozowski, J. Burzynski, A.M. Costa, C. Carissimo, R. Dimitrova, J. Franke, D. Grawe, I. Goricsan, A. Hellsten, Z. Janour, A. Karppinen, M. Ketzel, J. Krajcovicova, B. Leitl, A. Martilli, N. Moussiopoulos, M. Neophytou, H. Olesen, C. Papachristodoulou, M. Papadakis, M. Piringer, S. Di Sabatino, M. Sandberg, M. Schatzmann, H. Schlünzen and S. Trini-Castelli, (2007). Cost Action 732 Quality Assurance and Improvement of Microscale Meteorological Models. Brussels, Belgium.

Batt, R., S. Gant, J. Lacome and B. Truchot (2016). Modelling of Stably-Stratified Atmospheric Boundary Layers with Commercial CFD Software for use in Risk Assessment. *Chemical Engineering Transactions 48*, 61-66.

Bénard, P., A. Hourri, B. Angers and A. Tchouvelev (2016). Adjacent Surface Effect on the Flammable Cloud of Hydrogen and Methane Jets: Numerical Investigation and Engineering Correlations. *International Journal of Hydrogen Energy 41*, 18654-662.

Birch, A.D., D.R. Brown, M.G. Dodson and F. Swaffield (1984). The Structure and Concentration Decay of High-Pressure Jets of Natural Gas. *Combustion Science and Technology 36,* 249-261.

Busini, V., M. Lino and R. Rota (2012). Influence of Large Obstacles and Mitigation Barriers on Heavy Gas Cloud Dispersion: A Liquefied Natural Gas Case-Study. *Industrial and Engineering Chemistry Research 51*, 7643–50.

Busini, V. and R. Rota (2014). Influence of the shape of mitigation barriers on heavy gas dispersion. *Journal of Loss Prevention in the Process Industries 29*, 13-21.

Casal, J., M. Gomez-Mares, M. Munoz and A. Palacios (2012). Jet Fires: a "Minor" Fire Hazard? *Chemical Engineering Transactions 26*, 13-20.

Chen, C.J. and W. Rodi (1980). *Vertical Turbulent Buoyant Jets – A review of Experimental Data* (First ed.). Pergamon Press Vol. 4.

Colombini, C. and V. Busini (2019). Obstacle Influence on High-Pressure Jets based on Computational Fluid Dynamics Simulations. *Chemical Engineering Transactions 75*, in press.

Hall, J.E., P. Hooker, L. O'Sullivan, B. Angers, A. Hourri and P. Bernard (2017). Flammability Profiles Associated with High-Pressure Hydrogen Jets Released in Close Proximity to Surfaces. *International Journal of Hydrogen Energy 42*, 7413-21.

Houf, W., R. Schefer, G. Evans, E. Merilo and M. Groethe (2010). Evaluation of barrier walls for mitigation of unintended releases of hydrogen. *International Journal of Hydrogen Energy 35*, 4758-75.

Hourri, A., B. Angers and P. Bénard (2009). Surface Effects on Flammable Extent of Hydrogen and Methane Jets. *International Journal of Hydrogen Energy 34*, 1569-1577.

Middha, P., O.R. Hansen, J. Grune and A. Kotchourko (2010). CFD calculations of gas dispersion and subsequent gas explosions: Validation against ignited impinging hydrogen jet experiments. *Journal of Hazardous Materials 179*, 84-94.

Pontiggia, M., V. Busini, M. Ronzoni, G. Uguccioni and R. Rota (2014). Effect of Large Obstacles on High Momentum Jets Dispersion. *Chemical Engineering Transactions 36,* 523-528.

Zuliani, C., C. De Lorenzi and S. Ditali (2016). Application of CFD Simulation to Safety Problems – Challenges and Experience Including a Comparative Analysis of Hot Plume Dispersion from a Ground Flare. *Chemical Engineering Transactions 53,* 79-84.